Draft version February 27, 2018
Typeset using LaTeX **preprint** style in AASTeX61

CHARACTERISTICS AND ENERGY DEPENDENCE OF RECURRENT GALACTIC COSMIC-RAY FLUX DEPRESSIONS AND OF A FORBUSH DECREASE WITH LISA PATHFINDER

M. Armano,[1] H. Audley,[2] J. Baird,[3] M. Bassan,[4] S. Benella,[5,6] P. Binetruy,[7,*] M. Born,[2] D. Bortoluzzi,[8] A. Cavalleri,[9] A. Cesarini,[5] A. M. Cruise,[10] K. Danzmann,[2] M. de Deus Silva,[1] I. Diepholz,[2] G. Dixon,[10] R. Dolesi,[11] M. Fabi,[5] L. Ferraioli,[12] V. Ferroni,[11] N. Finetti,[6,13] E. D. Fitzsimons,[14] M. Freschi,[1] L. Gesa,[15] F. Gibert,[11] D. Giardini,[12] R. Giusteri,[11] C. Grimani,[5,6] J. Grzymisch,[16] I. Harrison,[17] G. Heinzel,[2] M. Hewitson,[2] D. Hollington,[3] D. Hoyland,[10] M. Hueller,[11] H. Inchauspé,[7] O. Jennrich,[16] P. Jetzer,[18] N. Karnesis,[2] B. Kaune,[2] N. Korsakova,[19] C. J. Killow,[19] M. Laurenza,[6,20] J. A. Lobo,[15,†] I. Lloro,[15] L. Liu,[11] J. P. López-Zaragoza,[15] R. Maarschalkerweerd,[17] D. Mance,[12] V. Martín,[15] L. Martin-Polo,[1] J. Martino,[7] F. Martin-Porqueras,[1] I. Mateos,[15] P. W. McNamara,[16] J. Mendes,[17] L. Mendes,[1] M. Nofrarias,[15] S. Paczkowski,[2] M. Perreur-Lloyd,[19] A. Petiteau,[7] P. Pivato,[11] E. Plagnol,[7] J. Ramos-Castro,[21] J. Reiche,[2] D. I. Robertson,[19] F. Rivas,[15] G. Russano,[11] F. Sabbatini,[5] J. Slutsky,[22] C. F. Sopuerta,[15] T. Sumner,[3] D. Telloni,[6,23] D. Texier,[1] J. I. Thorpe,[22] D. Vetrugno,[11] S. Vitale,[11] G. Wanner,[2] H. Ward,[19] P. Wass,[3] W. J. Weber,[11] L. Wissel,[2] A. Wittchen,[2] A. Zambotti,[8] C. Zenoni,[8] and P. Zweifel[12]

[1] *European Space Astronomy Centre, European Space Agency, Villanueva de la Cañada, 28692 Madrid, Spain*
[2] *Albert-Einstein-Institut, Max-Planck-Institut für Gravitationsphysik und Leibniz Universität Hannover, Callinstraße 38, 30167 Hannover, Germany*
[3] *High Energy Physics Group, Physics Department, Imperial College London, Blackett Laboratory, Prince Consort Road, London, SW7 2BW, UK*
[4] *Dipartimento di Fisica, Università di Roma "Tor Vergata" and INFN sezione Roma Tor Vergata, 00133 Roma, Italy*
[5] *DISPEA, Università di Urbino "Carlo Bo", Via S. Chiara, 27, 61029 Urbino, Italy*
[6] *INFN - Sezione di Firenze, via G. Sansone 1, 50019, Sesto Fiorentino, Firenze, Italy*
[7] *APC, Univ Paris Diderot, CNRS/IN2P3, CEA/lrfu, Obs de Paris, Sorbonne Paris Cité, France*
[8] *Department of Industrial Engineering, University of Trento, via Sommarive 9, 38123 Trento, and Trento Institute for Fundamental Physics and Application / INFN*
[9] *Istituto di Fotonica e Nanotecnologie, CNR-Fondazione Bruno Kessler, I-38123 Povo, Trento, Italy*
[10] *The School of Physics and Astronomy, University of Birmingham, Birmingham, UK*
[11] *Dipartimento di Fisica, Università di Trento and Trento Institute for Fundamental Physics and Application / INFN, 38123 Povo, Trento, Italy*
[12] *Institut für Geophysik, ETH Zürich, Sonneggstrasse 5, CH-8092, Zürich, Switzerland*
[13] *Dipartimento di Scienze Fisiche e Chimiche, Università degli Studi dell'Aquila, Via Vetoio, Coppito, 67100 L'Aquila, Italy*
[14] *The UK Astronomy Technology Centre, Royal Observatory Edinburgh, Blackford Hill, Edinburgh, EH9 3HJ, UK*
[15] *Institut de Ciències de l'Espai (CSIC-IEEC), Campus UAB, Carrer de Can Magrans s/n, 08193 Cerdanyola del Vallès, Spain*

Corresponding author: Catia Grimani
catia.grimani@uniurb.it

Institut d'Estudis Espacial de Catalunya (IEEC), Edifici Nexus I, C/ Gran Capità 2-4, despatx 201, E-08034 Barcelona, Spain
[16] *European Space Technology Centre, European Space Agency, Keplerlaan 1, 2200 AG Noordwijk, The Netherlands*
[17] *European Space Operations Centre, European Space Agency, 64293 Darmstadt, Germany*
[18] *Physik Institut, Universität Zürich, Winterthurerstrasse 190, CH-8057 Zürich, Switzerland*
[19] *SUPA, Institute for Gravitational Research, School of Physics and Astronomy, University of Glasgow, Glasgow, G12 8QQ, UK*
[20] *Istituto di Astrofisica e Planetologia Spaziali, INAF, Roma, Italy*
[21] *Department d'Enginyeria Electrònica, Universitat Politècnica de Catalunya, 08034 Barcelona, Spain*
[22] *Gravitational Astrophysics Lab, NASA Goddard Space Flight Center, 8800 Greenbelt Road, Greenbelt, MD 20771 USA*
[23] *Osservatorio Astrofisico di Torino, INAF, Pino Torinese, Italy*

Submitted to ApJ

ABSTRACT

Galactic cosmic-ray (GCR) energy spectra observed in the inner heliosphere are modulated by the solar activity, the solar polarity and structures of solar and interplanetary origin. A high counting rate particle detector (PD) aboard LISA Pathfinder (LPF), meant for subsystems diagnostics, was devoted to the measurement of galactic cosmic-ray and solar energetic particle integral fluxes above 70 MeV n^{-1} up to 6500 counts s^{-1}. PD data were gathered with a sampling time of 15 s. Characteristics and energy-dependence of GCR flux recurrent depressions and of a Forbush decrease dated August 2, 2016 are reported here. The capability of interplanetary missions, carrying PDs for instrument performance purposes, in monitoring the passage of interplanetary coronal mass ejections (ICMEs) is also discussed.

Keywords: cosmic rays — instrumentation: interferometers — interplanetary medium — Sun: rotation — Sun: heliosphere — solar-terrestrial relations

* Deceased 1 April 2017
† Deceased 30 September 2012

1. INTRODUCTION

Galactic cosmic-ray (GCR) flux observations in the heliosphere present long-term (> 1 year) and short-term (≤ 27 days) modulations. Both were extensively studied in the last 60 years on Earth with neutron monitors and in space (Forbush 1954, 1958; Storini, Iucci and Pase 1992; Beer 2000; Hajadas et al. 2004; Clem and Evenson 2004; Ferreira, Potgieter and Scherer 2004; Grimani 2004, 2007; Grimani et al. 2007; Shikaze et al. 2007; Sabbah and Kudela 2011; Usoskin, Bazilevskaya and Kovaltsov 2011; Laurenza et al. 2012, 2014; Usoskin et al. 2017).

Long-term variations are associated with the 11-year solar cycle and the 22-year solar polarity reversal. At solar maximum GCR energy spectra appear depressed by approximately one order of magnitude at 100 MeV n^{-1} with respect to similar observations gathered at solar minimum (see for instance Papini, Grimani and Stephens 1996, and references therein). Moreover, at solar minimum and during negative (positive) solar polarity periods, defined by the solar magnetic field directed inward (outward) at the Sun north pole, positively (negatively) charged particle fluxes are depressed by a maximum of 40% at 100 MeV n^{-1} with respect to measurements performed during opposite periodicities (Boella et al. 2001; Gil and Alania 2016). Positively charged particles propagate mainly sunward in the ecliptic along the heliospheric current sheet (HCS) during negative solar polarity periods and over the poles during positive polarity epochs. The opposite holds for negatively charged particles (Potgieter and Langner 2004; Ferreira 2005). Particles propagating along the HCS lose more energy than those coming from the poles (Strauss et al. 2011).

The most intense short-term GCR flux drops occur during classical, non recurrent, Forbush decreases (Forbush 1937; Cane 2000). These depressions are characterized by maximum GCR flux decreases of 30% at 100 MeV n^{-1} and are associated with the passage of interplanetary counterparts of coronal mass ejections. Recurrent depressions are caused by corotating high-speed solar wind streams (see Iucci et al. 1979, for instance). Quasi-periodicities of 27 days, 13.5 days and 9 days, correlated with the Sun rotation period (27.28 days for an Earth observer) and higher harmonics, are observed in the cosmic-ray flux, in the solar wind plasma, in the interplanetary magnetic field and in the geomagnetic activity indices (Čalogović et al. 2008; Emery et al. 2011). These investigations are typically carried out with neutron monitors that allow for long-term studies of the role of interplanetary structures in modulating the GCR flux (see for instance Simpson 1954; Gil and Alania 2010; Sabbah and Kudela 2011; Badruddin and Kumar 2016). A correlation of the GCR flux short-term variations with the BV product of the interplanetary magnetic field (IMF) intensity (B) and the solar wind speed (V) was investigated by Sabbah (2000). This approach takes into account both cosmic-ray diffusion from interplanetary magnetic field and convection in the solar wind. From the point of view of geomagnetic indices, a good correlation of A_p and K_p with both BV and BV^2, was found by Sabbah (2007). Depressions of the cosmic-ray flux were studied in space since the sixties (see for instance McCracken, Rao and Bukata 1966). Richardson, Wibberenz and Cane (1996) carried out an extensive campaign of observations of GCR flux short-term variations above a few tens of MeV aboard the Helios 1, Helios 2 and IMP-8 spacecraft. These observations indicated that the effects of corotating interaction regions (CIRs), generated when high-speed solar wind streams, associated with stable, low-latitude extensions of polar coronal holes, overtake leading slow solar wind from the equatorial regions of the Sun, are at the origin of short-term GCR flux modulations (see also Richardson 2004).

A high counting rate particle detector (PD; Cañizares et al. (2011)) hosted aboard the European Space Agency (ESA) LISA Pathfinder (LPF) mission (Antonucci et al. 2011, 2012; Armano et al. 2016), allowed for the monitoring of the integral proton and helium nucleus fluxes above 70 MeV n^{-1} (Araújo et al. 2005; Mateos et al. 2012) with statistical uncertainty at percent level on 1-hour binned data between February 2016 and July 2017.

The energy-dependence of GCR short-term depressions can be studied by exploiting the contemporaneous measurements of cosmic rays in space above a few tens of MeV with missions carrying PDs and on Earth with neutron monitors located at different geographic latitudes. GCR counting rates observed with neutron monitors vary proportionally to the cosmic-ray flux, thus providing a direct measurement of the same, at energies larger than the *effective energy* (Gil et al. 2017) which ranges between 11-12 GeV and above 20 GeV for near-polar and equatorial stations, respectively.

This paper reports on the characteristics of GCR flux periodicities and depressions observed during the Bartels rotations (BRs) 2490-2508 (from February 18, 2016 through July 3, 2017) after properly taking into account the effects of long-term variations. It is recalled here that the BR number corresponds to the number of 27-day rotations of the Sun since February 8, 1832. The years 2016-2017 were characterized by the presence of near-equatorial coronal holes and equatorward extensions of polar coronal holes, resulting in a very favourable period to carry out the study illustrated here. The energy-dependence of recurrent and non-recurrent GCR depressions is also investigated. In particular, it is reported on the characteristics of a classical Forbush decrease, a sudden depression of the GCR flux observed with LPF on August 2nd, 2016. This occurrence was associated with an increase of the IMF intensity due to the passage of an interplanetary coronal mass ejection (ICME; `http://www.srl.caltech.edu/ACE/ASC/DATA/level3/icmetable2.htm` and Richardson and Cane (2010)) that caused a geomagnetic disturbance of modest intensity started at 21.30 UT of the same day. GCR proton energy spectra in August 2016 before and at the deep of the depression are estimated and presented in this work. These observations indicate the value of interplanetary missions carrying particle detectors that, while primarily devoted to mission performance purposes, can also provide valuable measurements for space science and space weather studies (see also Hajadas et al. 2004; Lilensten 2007, and references therein).

This manuscript is organized as it follows: Section 2 describes the characteristics of the LPF mission. In Section 3 are presented the parameterizations of the proton and helium energy spectra during the LPF mission. In Section 4 and Section 5 are reported the characteristics and the energy dependence of the observed GCR flux short-term variations, respectively. Finally, in Section 6 it is discussed the capability of the LPF PD to monitor the passage of interplanetary coronal mass ejections.

2. LPF MISSION AND ORBIT

LPF was the technology demonstrator mission for LISA, the first space interferometer devoted to gravitational wave detection in the frequency range 10^{-4} Hz - 10^{-1} Hz (Armano et al. 2017a). The LPF spacecraft was launched from the Kourou base in French Guiana on December 3rd, 2015 aboard a Vega rocket. It reached its final orbit (which took approximately 6 months to complete) around the Earth-Sun Lagrangian point L1 at 1.5 million km from Earth at the end of January 2016. The LPF orbit was inclined at about 45 degrees with respect to the ecliptic plane. Orbit minor and major axes were approximately of 0.5 million km and 0.8 million km, respectively. The satellite spinned on its own axis in six months. The LPF satellite carried two, 2-kg cubic platinum-gold free-floating test masses that play the role of mirrors of the interferometer. Protons and ions of

galactic or solar origin with energies larger than 100 MeV n^{-1} penetrated or interacted in about 13 g cm^{-2} of spacecraft and instrument materials charging the LPF test masses. This charging process results in spurious noise forces on both test masses (Shaul et al. 2006; Armano et al. 2017b). A PD (Cañizares et al. 2011) was placed aboard LPF for *in situ* monitoring of GCR and solar particle overall flux. The LPF PD was mounted behind the spacecraft solar panels with its viewing axis along the Sun-Earth direction. It consisted of two $\sim$ 300 μm thick silicon wafers of 1.40 x 1.05 cm^2 area, placed in a telescopic arrangement at a distance of 2 cm. For particle energies $>$ 100 MeV n^{-1} the instrument geometrical factor was found to be energy independent and equal to 9 cm^2 sr for particle isotropic incidence on each silicon layer. When particles traversed both silicon wafers within 525 ns of each other (coincidence mode), the geometrical factor was about one tenth of this value. A shielding copper box of 6.4 mm thickness surrounded the silicon wafers. The shielding material stopped particles with energies smaller than 70 MeV n^{-1}. The PD allowed for the counting of protons and helium nuclei traversing each silicon layer (single counts) and for the measurement of ionization energy losses of particles in coincidence mode. The single counts were gathered with a sampling time of 15 s and ionization energy losses of events in coincidence mode were stored in the form of histograms over periods of 600 seconds and then sent to the on-board computer. The maximum allowed detector counting rate was 6500 counts s^{-1} on both silicon wafers, corresponding to an event integrated proton fluence of 10^8 protons cm^{-2} at energies $>$ 100 MeV. In coincidence mode 5000 energy deposits per second was the saturation limit. The occurrence of SEP events with fluences larger than the saturation limit was estimated to be less than one per year for the period the LPF spacecraft remained into orbit around L1 (Nymmik 1999a,b; Grimani et al. 2012). As a matter of fact, no SEP events characterized by a proton differential flux above a few tens of MeV n^{-1} overcoming that of galactic origin were observed during the period of the LPF mission operations considered for this analysis.

3. GALACTIC COSMIC-RAY PROTON AND HELIUM NUCLEUS ENERGY SPECTRA DURING THE LPF MISSION

The LPF 15-s proton (p) and helium (He) single counts gathered between mid-February 2016 and July 3, 2017 were hourly-averaged in order to limit the statistical uncertainty on the measurements to 1% (see Fig. 1). Observations were interrupted only for brief, planned system resets. The GCR count rate appears modulated on time scales of several days and presents an increasing trend over the mission lifetime due to a decreasing level of the solar activity. It is worthwhile to recall that LPF was sent into orbit during the descending phase of the solar cycle N° 24 under a positive polarity period. In Grimani et al. (2007) it was shown that during positive polarity periods the energy spectra, $J(r, E, t)$, of cosmic rays at a distance r from the Sun and at a time t, are well represented by the symmetric model in the *force field approximation* by Gleeson and Axford (G&A; Gleeson and Axford (1968)) assuming time-independent interstellar intensities $J(\infty, E + \Phi)$ and an energy loss parameter Φ:

$$\frac{J(r, E, t)}{E^2 - E_0^2} = \frac{J(\infty, E + \Phi)}{(E + \Phi)^2 - E_0^2} \tag{1}$$

where E and E_0 represent the particle total energy and rest mass, respectively. For Z=1 particles with rigidity (particle momentum per unit charge) larger than 100 MV, the effect of the solar activity is completely defined by the *solar modulation parameter* ϕ that, at these energies, is equal to Φ (see also Grimani et al. 2009).

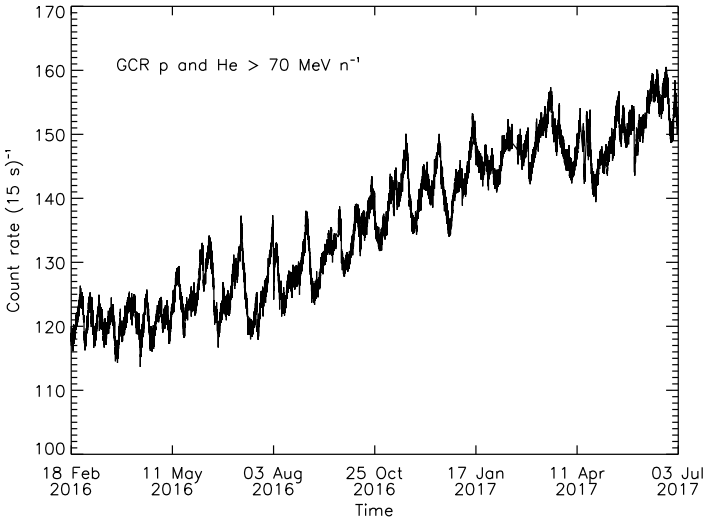

Figure 1. Fifteen second hourly-averaged GCR single count rate observed with the PD aboard the LPF mission.

The solar modulation parameter for the first year of the LPF mission (December 2015 - December 2016) was taken from http://cosmicrays.oulu.fi/phi/Phi_mon.txt (see also Usoskin, Solanki and Korte 2006). For the same period, the GCR single counts per sampling time of 15 seconds, averaged over each BR (GCR_{15s}), were calculated. A linear correlation was found between the solar modulation parameter ϕ and GCR_{15s}:

$$GCR_{15s} = -0.23272\ \phi(MV) + 230.73 \tag{2}$$

as it is shown in Fig. 2 at the right side of the dashed line, indicated by *DATA*. This observation suggests that the LPF PD did not present any detectable loss of efficiency during the first year of the mission lifetime. Therefore, the same was reasonably assumed for the last six months of mission operations. Projections of the solar modulation parameter for the year 2017 (for which estimates are not available in http://cosmicrays.oulu.fi/phi/Phi_mon.txt) were carried out by extrapolating the same trend shown by GCR_{15s} and ϕ in 2016 (see Fig. 2 at the left of the dashed line indicated by *PROJECTIONS*). The observed PD single count rate increased by more than 20% during the LPF mission due to a decreasing solar activity. The monthly sunspot number (http://www.sidc.be/silso/home) was observed to decrease smoothly from 58 to 18.5 during the first year of the LPF mission while from January 2017 through the beginning of July 2017 the sunspot number did not change appreciably varying from 26.1 to 19.4. Therefore, the value of ϕ assumed here at the end of the LPF mission can be considered a lower limit.

The proton and helium energy differential fluxes at the beginning (December 2015 - January 2016; ϕ=550 MV) and at the end (July 2017; ϕ=320 MV) of the LPF mission were estimated with the model by G&A by using the proton and helium energy spectra at the interstellar medium obtained from a series of balloon flights of the BESS and BESS-Polar experiments (see Shikaze et al. 2007; Abe et al. 2016, for details). The BESS, BESS-Polar and other balloon-borne experiment data gathered during different periods of solar activity and solar polarity, are reported in Fig. 3. In this figure open (solid) symbols indicate data gathered during positive (negative) polarity periods. In Grimani et al. (2004)

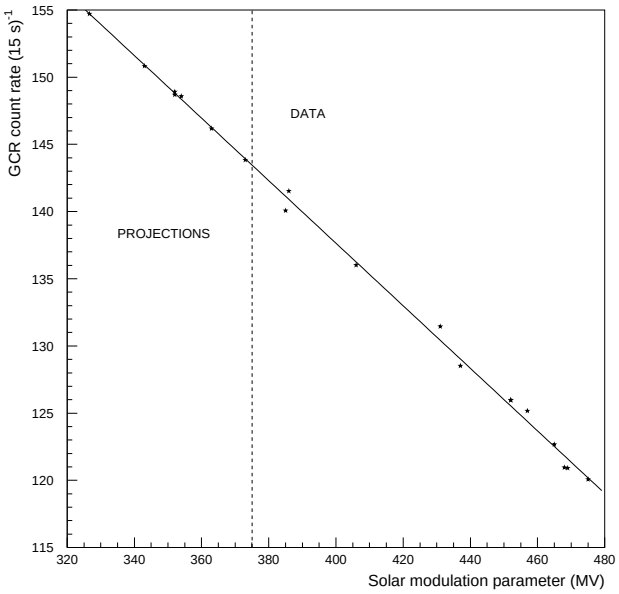

Figure 2. Solar modulation parameter and LPF PD GCR single count rate in 15 s sampling time averaged over each BR during the LPF mission. High (low) values of the solar modulation parameter correspond to mission beginning (end). See text for details. Estimates of the solar modulation parameter up to December 2016 appear in http://cosmicrays.oulu.fi/phi/Phi_mon.txt. In 2017 projections of the solar modulation parameter were carried out on the basis of the parameterization appearing as a continuous line and reported in equation (2).

and references therein it was shown that contemporaneous observations of GCR fluxes in the inner heliosphere show variations of $\sim 3\%$ AU^{-1} and 0.33% per latitude degree off the ecliptic. It can be concluded that particle spectra at the interstellar medium obtained with data gathered near Earth can also be used for LPF which orbited at just 0.01 AU from Earth. Finally, the interstellar spectra by BESS-BESS-Polar were privileged in this work since they were inferred from proton and helium observations gathered during conditions of solar activity and solar polarity similar to those of LPF.

The energy spectra, F(E), obtained with the G&A model for LPF were interpolated with the function appearing in equation 3, which is well representative of the GCR observations trend in the inner heliosphere between a few tens of MeV and hundreds of GeV within experimental errors (see for details Papini, Grimani and Stephens 1996):

$$F(E) = A\ (E+b)^{-\alpha}\ E^{\beta} \quad \text{particles (m}^2\text{ sr s GeV n}^{-1})^{-1}, \tag{3}$$

where E is the particle kinetic energy per nucleon. The parameters A, b, α and β were estimated for proton and helium nucleus energy spectra at the beginning and at the end of the LPF mission and reported in Table 1. The energy spectra obtained here for the beginning of the LPF mission (dot-dashed curve in Fig. 3; ϕ=550 MV) lie, as expected, between the BESS97 (ϕ=491 MV) and the BESS98 (ϕ=591 MV) data, gathered during a positive polarity period. In the same figure maximum projections of proton and helium energy spectra at the end of the LPF mission appear as continuous lines. The same value of ϕ was used for both proton and helium energy spectra estimates.

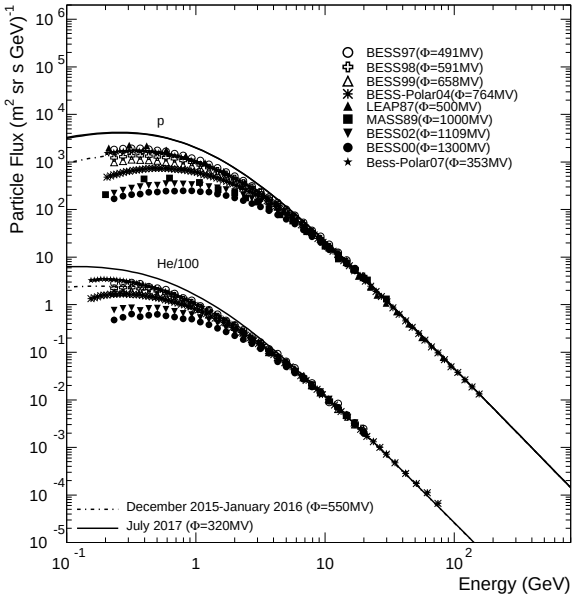

Figure 3. GCR proton and helium energy spectra measurements (Shikaze et al. 2007, and references therein). Estimated energy spectra at the beginning (December 2015 - January 2016) at the end of the LPF mission (July 2017) are also indicated as dot-dashed and continuous lines, respectively. The helium flux appears properly scaled in order not to superpose lines.

Table 1. Parameterizations of proton and helium energy spectra at the beginning and at the end of the LPF mission according to the function $F(E) = A\ (E + b)^{-\alpha}\ E^{\beta}$ particles (m^2 sr s GeV n^{-1})$^{-1}$

	A	b	α	β
p (Dec. 2015 - Jan. 2016)	18000	1.19	3.66	0.87
p (July 2017)	18000	0.82	3.66	0.87
He (Dec. 2015 - Jan. 2016)	850	0.96	3.23	0.48
He (July 2017)	850	0.68	3.23	0.48

4. OBSERVATIONS OF GCR FLUX SHORT-TERM VARIATIONS ABOARD LPF

The power spectral density (PSD) from the Lomb-Scargle (LS; Lomb (1976); Scargle (1982)) periodogram analysis of the whole LPF GCR data sample adopted for this study is shown in Fig. 4. The LS periodogram technique is used here to retrieve the periodicities of galactic cosmic-ray modulation. Fig. 4 shows that periodicities of 9 days, 13.5 days and 27 days correlated to the Sun rotation and higher harmonics periodicities are present in the whole GCR PD data. In order to assess

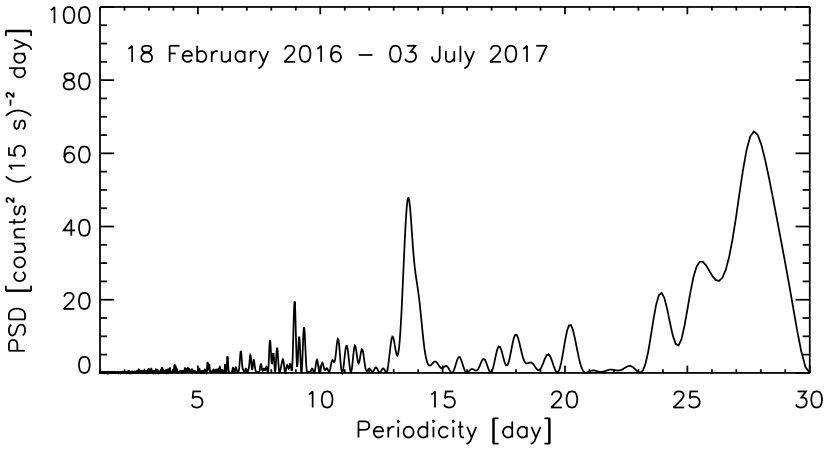

Figure 4. Power spectral density from the Lomb-Scargle periodogram analysis applied to the whole LPF PD data set adopted in this work. Sun rotation and higher harmonics periodicities are dominant.

the time variability of these dominant periodicities, the period of observations was divided in three sub-intervals, each encompassing about four months and a half.

The corresponding LS power spectral densities are displayed in Fig. 5. The 9-day and 13.5-day periodicities are strongly modulated in time and progressively damped, with the former being the first to disappear. The periodicity related to the Sun rotation is present during the whole observational period, though its value slightly changes in time from about 27 days (middle panel) to 31 days (third panel).

In order to study the occurrence and the characteristics of individual GCR flux short-term depressions, the LPF PD observations during each BR were compared to interplanetary magnetic field, solar wind plasma parameters and to neutron monitor measurements. Moreover, data gathered during each Bartels rotation were compared by eye to those observed during previous and subsequent Bartels rotations in order to detect the presence of recurring and non-recurring patterns in the variation of GCR data and solar wind parameters.

The effects of the decrease of the solar activity over the mission were reduced by considering the fractional variations of the cosmic-ray flux with respect to the average value during each BR. The same approach was considered in Wiedenbeck et al. (2009) for the ACE experiment in L1. Forty-four recurrent depressions and one classical Forbush decrease were observed. The commencement of individual depressions was set at the beginning of each continuous decrease of the GCR flux observed for more than 12 hours. GCR flux depressions with duration > 1 day and amplitude $> 1.5\%$ were considered for this analysis. Small increases and depressions ($< 1.5\%$ in amplitude) lasting less than one day were at the limit of statistical significance and therefore were disregarded by interpolating the data trend. In the top panel of Fig. 6 the cosmic-ray flux fractional variations during the BR 2491 (from March 4, 2016 through March 30, 2016) present four depressions (according to the definition reported above) starting on March 5, March 12, March 23 and March 29, respectively. The small deeps on March 11-12 and March 19-20 along with the small increase on March 16-17 are neglected. The solar wind plasma speed appears in the second panel of Fig. 6. The IMF radial component is shown in the third panel and the IMF intensity in the fourth panel. In the third panel of Fig. 6 the HCS crossing (taken from http://omniweb.sci.gsfc.nasa.gov./html/polarity/polarity_

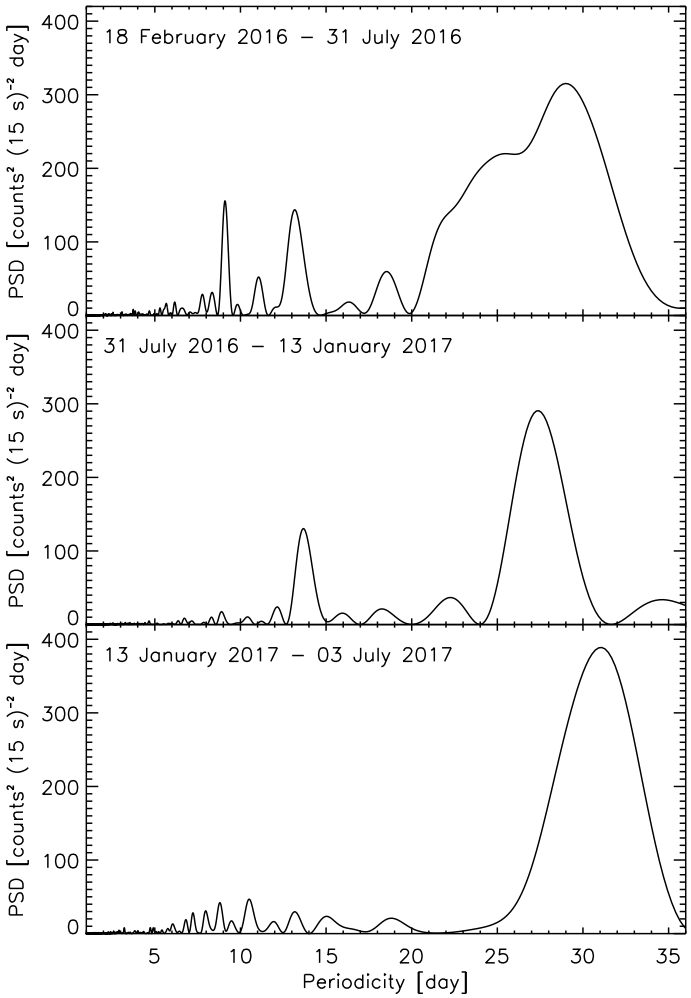

Figure 5. Power spectral density from the Lomb-Scargle periodogram analysis applied to the PD data gathered in the time interval indicated in each panel (which refers to one third of the whole LPF PD data set). Sun rotation and higher harmonics periodicities are modulated throughout the observational period.

tab.html) is also indicated. Solar wind plasma and IMF data are taken from the ACE experiment. The GCR flux depressions appear associated with those periods of time during which the solar wind plasma speed (V) is > 400 km s^{-1} and/or the IMF intensity (B) is > 10 nT (second and fourth panels in Fig. 6). This scenario basically corresponds to the passage of high-speed solar wind streams and/or CIRs (Harang 1968; Storini 1990; Cane, Richardson and von Rosenvinge 1995; Simpson 1998; McKibben et al. 1999; Bazilevskaya 2000). When GCR short-term variations are correlated with the BV parameter, the role of the magnetic field trend is privileged with respect to that of the solar wind speed since the IMF variations are larger than those of the solar wind speed. The GCR depressions observed with LPF are associated with solar wind speed changes smaller than 30% while the magnetic field is observed to increase up to a factor of 5. Therefore, a separate analysis of B and V increases helps in better understanding the dynamics of individual depressions resulting from the interplay of several interplanetary structures which affect the role of different periodicities during the mission as observed in Figs 4 and 5. From the point of view of time profiles of individual depressions, those presenting similar durations for decrease and recovery phases are called *symmetric*. All the other

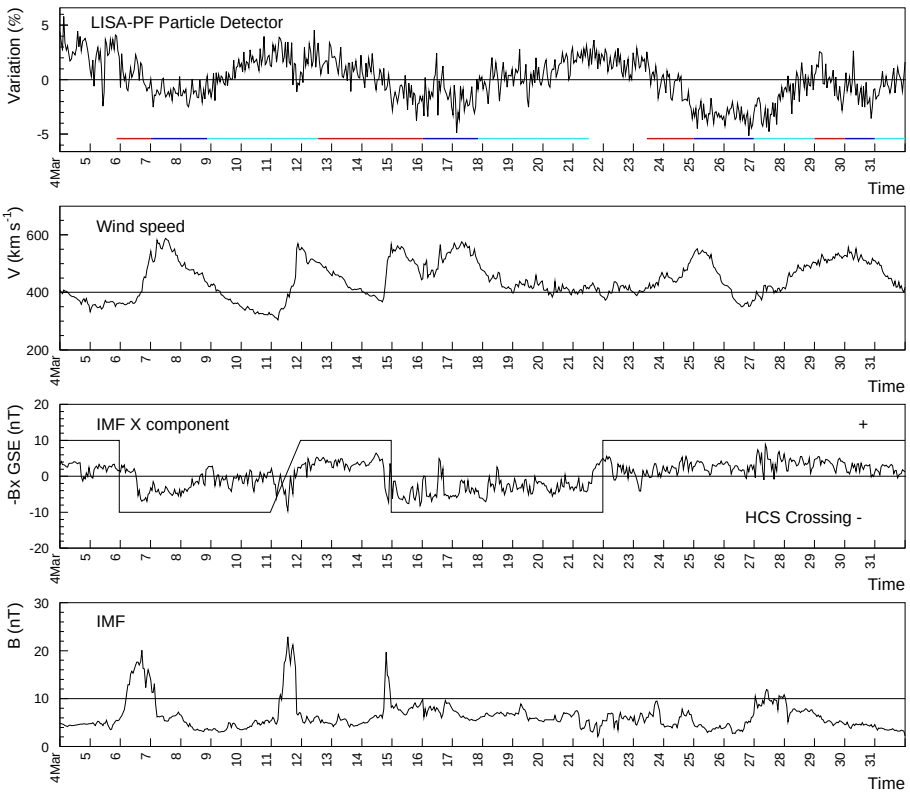

Figure 6. LPF PD counting rate fractional variations during the BR 2491 (March 4, 2016 - March 30, 2016)(first panel). Solar wind speed (second panel), IMF radial component (third panel) and IMF intensity (fourth panel) contemporaneous measurements, gathered by the ACE experiment, are also shown. HCS crossing (http://omniweb.sci.gsfc.nasa.gov./html/polarity/polarity_tab.html) is shown in the third panel. Periods of time during which the solar wind speed (V) and the magnetic field (B) intensity remain below and above 400 km s^{-1} and 10 nT, respectively, are shown in the second and fourth panels. Decrease, plateau and recovery periods of each GCR depression are represented by red, blue and cyan lines in the first panel.

depressions are called *asymmetric* (Badruddin and Singh 2006). The symmetric variations are V or U shaped. Thirty-nine out of forty-five depressions were found asymmetric. Only six appeared symmetric, and out of these, five were found U-shaped and only one V-shaped. The period during which the PD counting rate remained at minimum values between decrease and recovery phases is called here *plateau*. A plateau is observed during both U-shaped symmetric and asymmetric depressions and appears correlated with the period the solar wind velocity remains above 400 km s^{-1}. A typical asymmetric depression is that appearing in the top panel of Fig. 6 starting on March 5, 2016 with 2-day decrease, $\sim$ 1.5-day plateau and 3.5-day recovery periods. In the same figure a symmetric, U-cup-shaped depression starts on the 23rd of March with decrease, plateau and recovery phases lasting about 2 days each. Decrease, plateau and recovery phases for each depression during the Bartels rotation 2491 are shown in colors in the top panel of Fig. 6, as an example. Occurrence, characteristics and association with interplanetary structures of all depressions are summarized in Table 2. The GCR flux depressions that commence at the interaction regions of slow and fast solar

wind are associated to CIR in Table 2. Depressions observed to commence during different phases of corotating high speed solar wind stream passage are indicated by CHSS. HCS crossing (HCSC) and ICMEs are observed to play a minor role in modulating the GCR flux with respect to corotating high speed solar wind streams during the LPF mission. In Table 2 MFE (magnetic field enhancement) indicates a magnetic structure present in the slow solar wind. The association among magnetic structures and GCR flux depressions was carried out on the basis of contemporaneous interplanetary magnetic field and solar wind parameter observations from the ACE experiment.

Table 2. Occurrence and characteristics of the GCR flux depressions observed during the LPF mission. Interplanetary structures associated with the depressions are indicated (CIR: corotating interaction region; CHSS: corotating high-speed solar wind streams; ICME: interplanetary coronal mass ejection (http://www.srl.caltech.edu/ACE/ASC/DATA/level3/icmetable2.htm); S: shock; MC: magnetic cloud; HCSC: heliospheric current sheet crossing; MFE: magnetic field enhancement in the slow solar wind).

Date	Onset Time	Decrease Days	Plateau Days	Recovery Days	Amplitude %	Interplanetary structure
February 26, 2016	16.00 UT	2.5	1.0	3.2	7.0	CHSS
March 5, 2016	21.00 UT	2.0	1.0	3.5	4.9	ICME+CHSS
March 12, 2016	00.00 UT	3.5	2.0	3.5	5.3	CHSS
March 23, 2016	11.00 UT	2.0	2.0	2.0	6.0	CHSS
March 29, 2016	03.00 UT	1.0	1.0	4.0	3.4	CHSS
April 10, 2016	11.00 UT	4.0	0.0	5.5	3.1	MFE+HCSC+ICME
April 20, 2016	12.00 UT	3.0	2.0	4.5	7.1	CHSS
May 1, 2016	11.00 UT	1.5	1.0	2.0	2.8	CHSS
May 6, 2016	00.00 UT	2.8	0.0	6.5	4.7	CHSS
May 15, 2016	12.00 UT	4.0	1.0	1.0	7.2	CIR
May 29, 2016	13.00UT	1.5	0.0	5.0	3.0	CHSS
June 5, 2016	04.00 UT	1.0	1.0	4.0	5.1	CIR
June 12, 2016	07.00 UT	3.5	0.0	10.0	8.4	CHSS
June 30, 2016	07.00 UT	1.0	4.0	4.5	2.5	MFE+HCSC
July 7, 2016	00.00 UT	6.0	1.0	3.0	11.9	CIR
July 20, 2016	07.00 UT	1.0	1.0	12.0	5.4	ICME+CHSS
August 2, 2016	12.00 UT	1.0	0.0	2.8	9.0	ICME (S,MC)+ CHSS
August 5, 2016	21.00 UT	5.0	4.0	15.0	6.8	CHSS
August 29, 2016	21.00 UT	6.0	2.0	19.0	8.6	CIR

Table 2 continued on next page

Table 2 *(continued)*

Date	Onset Time	Decrease Days	Plateau Days	Recovery Days	Amplitude %	Interplanetary structure
September 26, 2016	12.00 UT	3.0	2.0	8.0	6.9	CIR
October 11, 2016	15.00 UT	2.0	0.0	2.0	5.0	HCSC+ICME
October 16, 2016	15.00 UT	1.0	0.0	5.5	2.8	CHSS
October 23, 2016	00.00 UT	6.0	2.0	8.0	7.5	CHSS
November 12, 2016	00.00 UT	1.0	3.0	4.0	1.6	CIR
November 20, 2016	16.00 UT	5.0	3.5	5.0	8.1	HCSC+CHSS
December 5, 2016	00.00 UT	1.0	1.0	1.0	1.9	MFE
December 7, 2016	12.00 UT	2.0	3.5	4.5	2.8	CIR
December 17, 2016	19.00 UT	8.5	1.0	4.5	10.9	CHSS
January 5, 2017	03.00 UT	1.0	2.0	6.5	3.0	CIR
January 14, 2017	15.00 UT	5.0	2.0	2.0	6.3	HCSC + CHSS
January 25, 2017	11.00 UT	2.5	0.0	3.0	3.4	HCSC + CHSS
January 30, 2017	16.00 UT	3.0	0.0	10.5	4.4	CIR
February 16, 2017	23.00 UT	1.0	1.0	2.5	3.1	CIR
February 23, 2017	10.00 UT	1.0	0.0	3.0	1.8	CIR
March 1, 2017	05.00 UT	2.0	0.0	5.5	3.9	CIR
March 21, 2017	00.00 UT	2.0	1.0	2.0	4.4	CIR
March 27, 2017	00.00 UT	8.0	3.5	5.5	6.9	CIR
April 18, 2017	09.00 UT	1.5	0.5	1.0	3.4	CIR
April 21, 2017	11.00 UT	3.0	2.0	4.5	7.8	CIR
May 1, 2017	00.00 UT	1.5	1.0	11.0	1.3	HCSC
May 15, 2017	08.00 UT	1.5	1.0	2.0	3.8	CIR
May 19, 2017	10.00 UT	1.5	1.0	5.5	2.5	HCSC+CHSS
May 27, 2017	18.00 UT	1.0	1.0	9.0	5.6	ICME (S)
June 12, 2017	16.00 UT	6.0	2.0	2.5	3.4	CHSS
June 24, 2017	14.00 UT	4.0	1.0	2.0	5.3	CIR

Average durations of decrease, plateau and recovery periods for the forty-five GCR depressions observed with LPF are reported in Table 3.

The average GCR flux depression amplitude of 5.1±2.5% appears consistent, within statistical errors, with that reported by Richardson (2004) of 3.2±0.1% for particle nominal energies larger than 60 MeV. The cut-off energy of particles observed with Helios I, Helios 2 and IMP8 was poorly estimated (Richardson 2004) while for the LPF PD observations the same was set with both Monte Carlo simulation and beam test experiment (Araújo et al. 2005; Mateos et al. 2012). However, since

Table 3. Average characteristics of GCR flux depressions observed with LPF.

	Duration (Days)	(%)
Decrease	2.8 ± 2.0	
Plateau	1.3 ± 1.2	
Recovery	5.1 ± 3.8	
Total duration	9.2 ± 5.0	
Intensity		5.1 ± 2.5

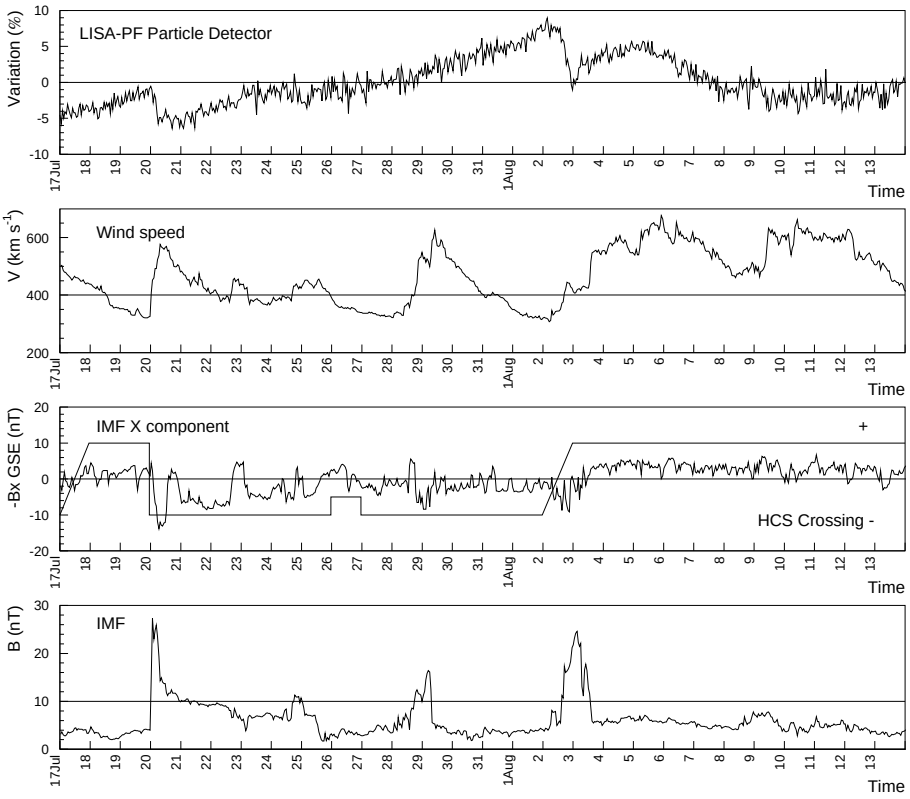

Figure 7. Same as Fig. 6 for the BR 2496 (July 17, 2016 - August 12, 2016).

the majority of cosmic-ray particles lie in the energy range of hundreds of MeV, a slightly difference in the detection capability of low energy particles is not expected to make a relevant difference for the above comparison.

The full evolution of one classical, two-step Forbush decrease (Cane 2000) was detected aboard LPF on August 2, 2016 as it is shown in Fig. 7. In this figure all panels are the same as in Fig. 6. The sharp decrease of the GCR flux on the 2nd of August lasted about 10 hours after 12.00 UT, no plateau was observed and the recovery period was modulated by an incoming high speed

solar wind stream. The GCR depression appears correlated with a contemporaneous increase of the interplanetary magnetic field intensity up to 24 nT, while the solar wind speed barely passed 400 km s^{-1}.

5. ENERGY-DEPENDENCE OF GCR FLUX SHORT-TERM DEPRESSIONS

Some clues are reported in the literature about the energy dependence of GCR flux short-term depressions. The energy-dependence of 27-day GCR flux variations, for instance, is discussed in Grimani et al. (2015) and references therein. The shielding effect of the atmosphere and the geomagnetic cut-off prevent neutron monitors to carry out a direct measurement of cosmic-ray energy spectra below effective energies of several GeV, although they can be obtained by using models combined with neutron monitors observations (Hofer and Flückiger 2000; Beer 2000; Usoskin, Bazilevskaya and Kovaltsov 2011; Usoskin et al. 2017). Interesting attempts to investigate the energy-dependence of short-term depressions of cosmic-ray fluxes above a few tens of MeV, through direct measurements with magnetic spectrometers, were carried out by the balloon-borne experiment BESS-Polar I (Thakur et al. 2011) and the satellite experiment PAMELA (Adriani et al. 2011). BESS-Polar I flew from Williams Field near Mc Murdo Station from December 13, 2004 through December 21, 2004. At the beginning of the flight, this balloon-borne experiment observed a recovering proton flux from a previous decrease. The recovery intensity appeared to be of 8-9% below 0.86 GeV and of 3% above 6 GeV. The authors claimed that this occurrence was due to the transit of a CIR interface or a magnetic cloud (Burlaga et al. 1981) or a combination of the two. This experiment detected a new GCR proton flux depression after the passage of a high-speed solar wind stream on December 17, 2004. The PAMELA experiment carried out the first measurement of proton and helium nucleus differential fluxes in space during a Forbush decrease on December 14, 2006 (16.50 UT-22.35 UT) after two SEP events dated December 13, 2006 and December 14, 2006. Unfortunately, balloon-borne magnetic spectrometer experiments, like BESS-Polar I, have short duration and space-borne instruments, like PAMELA, have small geometrical factors and therefore data must be integrated over periods longer than the typical one-hour data binning required to study recurrent GCR depressions.

The GCR flux fractional variations observed with the LPF PD have been compared to contemporaneous similar measurements carried out with neutron monitors placed at different geographic latitudes. Location, vertical cut-off rigidities and effective energies for all neutron monitor stations considered in this work are reported in Table 4. Both LPF PD and neutron monitor data were hourly averaged and appear in Figs. 8 and 9 for the BRs 2491 and 2496, respectively, as an example. This comparison indicates that while the maximum and average GCR fractional variations observed with LPF above 70 MeV n^{-1} are of more than 11% and of about 5%, respectively, the same goes down to a maximum of 3% above 11-12 GeV in near-polar stations and to a maximum of 2% above 15 GeV at increasing latitudes.

During the Forbush decrease observed on August 2, 2016 on LPF, a 3-σ decrease of the GCR flux occurred between 12.00 UT and 16.00 UT. The GCR flux reached its minimum at 22.40 UT: data indicated a GCR flux fractional decrease of 9% in L1 in $\sim$ 10 hours. The GCR flux depression recovered soon after the deep. The trend of this GCR flux depression appears different from recurrent GCR flux variations observed to be of 2% - 3% day^{-1} and 1% - 2% day^{-1} during the decrease and recovery periods, respectively. In Fig. 9 it can be noticed that the amplitude of the same depression is found to be of 3% in near-polar Terre Adelie and Oulu stations while it is of just 2% and 1% in

Table 4. Neutron monitor station location and characteristics.

Station	Location	Vertical cut-off rigidity GV	Effective Energy GeV
Thule	North Pole	0.3	11-12
Terre Adelie	South Pole	0.0	11-12
Mc Murdo	South Pole	0.3	11-12
Oulu	Finland	0.8	12
Rome	Italy	6.3	17
Mexico	Mexico	8.2	20

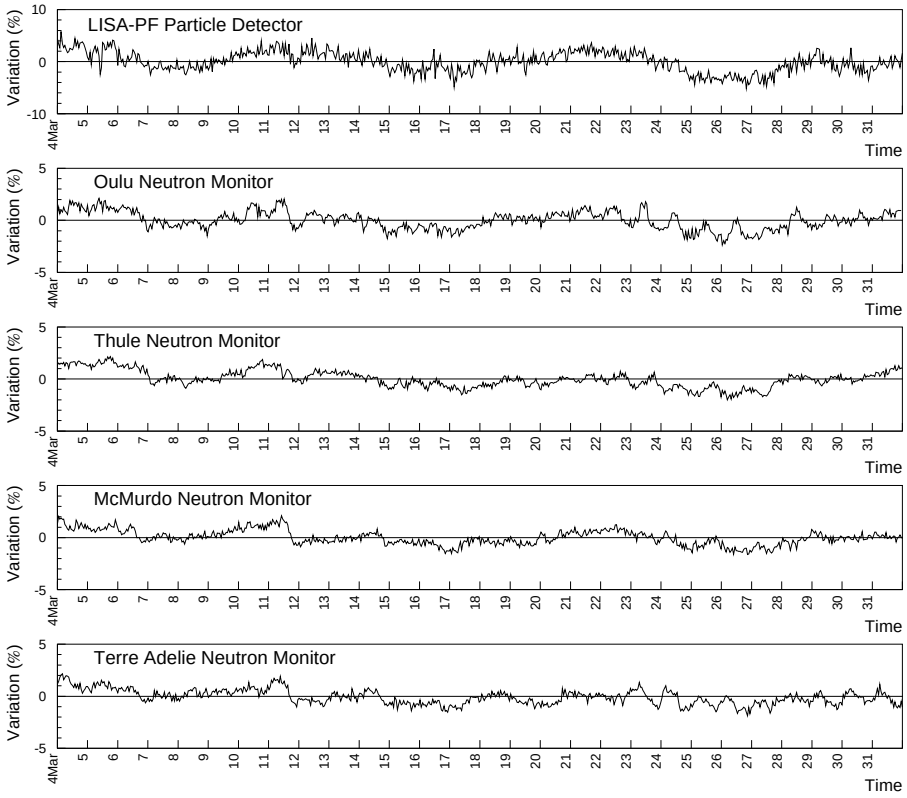

Figure 8. Comparison of LPF PD counting rate fractional variations with contemporaneous, analogous measurements of polar neutron monitors during the BR 2491 (March 4, 2016 - March 31, 2016).

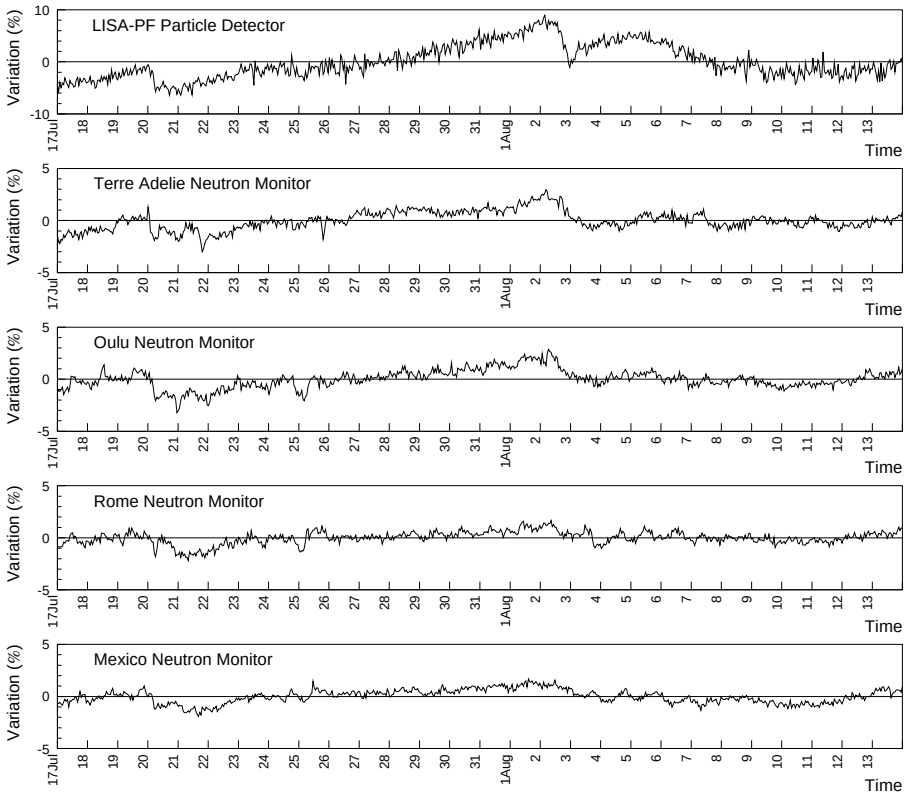

Figure 9. Comparison of LPF PD counting rate fractional variations with contemporaneous, analogous measurements of neutron monitors placed at various geographic latitudes during the BR 2496 (July 17, 2016 - August 13, 2016).

Rome and Mexico stations, respectively. In order to determine the GCR proton energy differential flux at the deep of the depression at 22.40 UT on LPF, the proton energy differential flux for the month of August 2016 (ϕ=438 MV) was estimated first above 70 MeV and parameterized following equation 3, as described in Section 3. The proton integral flux in August 2016 was then calculated as a integral of this differential flux. The proton integral flux, thus obtained, was properly reduced at 70 MeV as indicated by the LPF PD data and at the effective energy of each neutron monitor (reported in Table 4) on the basis of the neutron monitor decreases. Finally, the differential flux was inferred from the integral flux. The proton differential flux in August 2016 before the Forbush decrease and that estimated at the deep of the depression at 22.40 UT on August 2, 2016 were parameterized as reported in Table 5 and are compared in Fig. 10.

The helium differential flux at the deep of the depression was not estimated since no accurate proton-helium separation was allowed by the PD aboard LPF and the data trend is biased by protons since the He/p ratio in GCRs is about 0.1.

Measurements of the energy dependence of GCR flux recurrent and non recurrent depressions and the study of their evolution can be used to estimate the test-mass charging aboard future generation LISA-like interferometers (Grimani et al. 2015, and references therein). Despite minor changes in the instrument performance due to GCR short-term variations are expected, future interferometers

Table 5. Parameterizations of proton energy spectra for August 2016 before (continuous line in Fig. 10) and at the deep of the GCR depression observed on the 2nd of August (dotted line in Fig. 10).

	A	b	α	β
p (August 2016)	18000	1.01	3.66	0.87
p (August 2nd, 2016; depressed)	18000	1.068	3.66	0.869

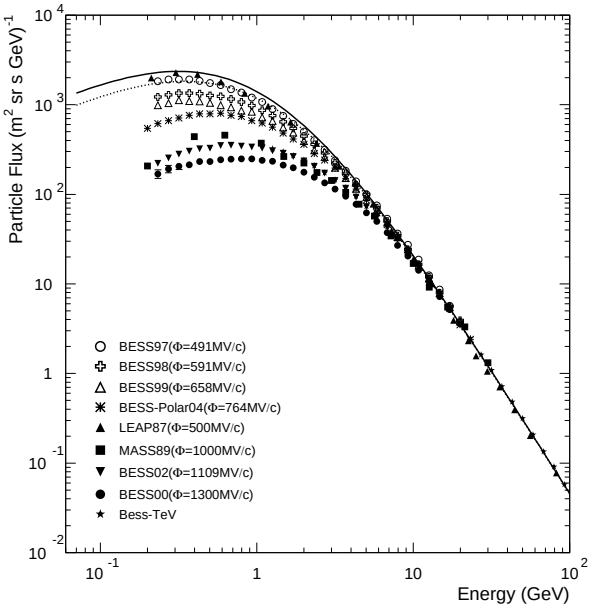

Figure 10. GCR proton energy spectra measurements and projections before (continuous line) and at the deep (dotted line) of the depression observed on August 2, 2016 with LPF.

devoted to gravitational wave detection in space will detect sub-femto-g spurious acceleration at low frequencies ($\sim 10^{-5}$ Hz), and the role of any interplanetary disturbance must be evaluated and quantified.

6. CAPABILITY OF THE LPF PD IN MONITORING THE PASSAGE OF INTERPLANETARY CORONAL MASS EJECTIONS

In this Section it is evaluated the capability of space missions like LPF, carrying PDs optimized for GCR detection, in monitoring the passage of ICMEs and in forecasting geomagnetic activity, when these interplanetary structures present intense southward magnetic field that reconnect with the Earth magnetic field and induce geomagnetic activity.

In Fig. 11 the Forbush decrease observed with LPF on the 2nd of August 2016 is compared to the contemporaneous IMF intensity and solar wind speed measured by ACE. The transit of an ICME near Earth from August 2, 2016 at 14.00 UT and August 3, 2016 at 3.00 UT, is indicated in the same figure by dashed lines (http://www.srl.caltech.edu/ACE/ASC/DATA/level3/icmetable2.htm; Richardson and Cane (see also 2010)). A detailed description of the characteris-

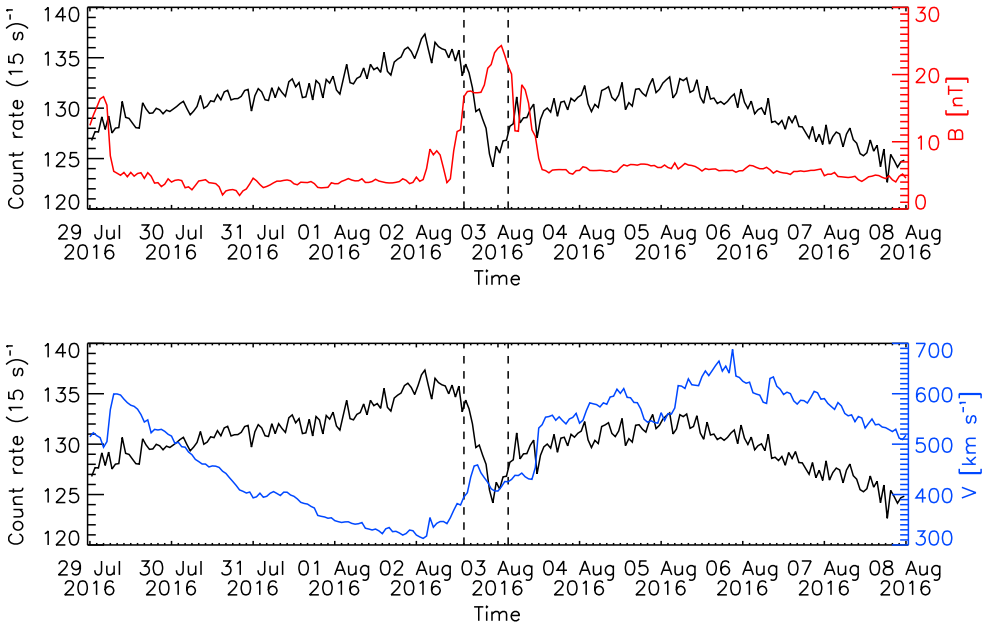

Figure 11. Comparison of the LPF PD counting rate fractional variations with IMF intensity (red line, right scale in the top panel) and solar wind speed (blue line right scale in the bottom panel) between July 29, 2016 and August 8, 2016. The vertical dashed line represent the beginning of the GCR flux depression observed with LPF and the passage of an ICME.

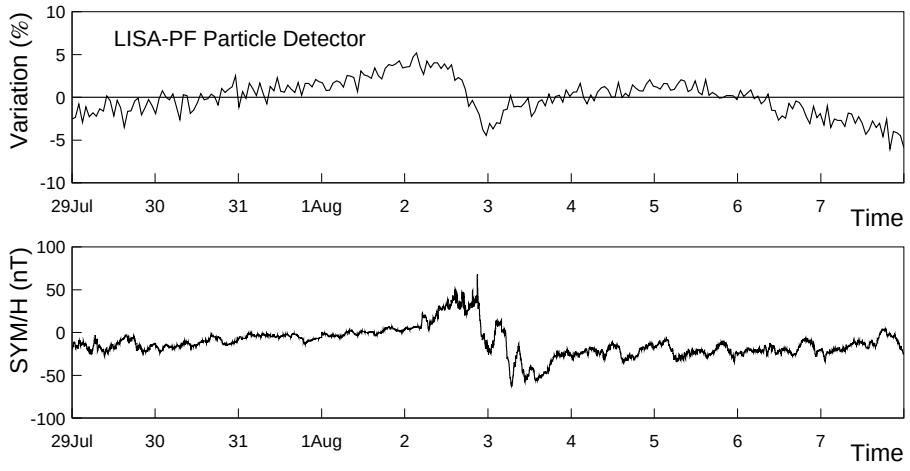

Figure 12. Comparison of the LPF PD counting rate fractional variations with the geomagnetic index SYM-H for the same period indicated in Fig. 11.

tics of this ICME is reported in http://www.stce.be/esww14/contributions/public/S4-P1/S4-P1-08-BenellaSimone/Poster_ESWW.pdf.

The decrease phase of the cosmic-ray flux seems to occur in two steps, suggesting that LPF crossed the region of the shock of the ICME and then the ejecta (Cane 2000). A geomagnetic disturbance was observed to start ($K_p > 5$) after 21.30 UT. In Fig. 12 the LPF GCR flux fractional variations are also compared to the SYM-H geomagnetic index which allows to follow the evolution of a geomagnetic disturbance at low latitudes. The characteristics of each GCR short-term flux depression are unique, often resulting from the interplaying effects of consecutive structures propagating in the interplanetary medium. However, for the August 2, 2016 Forbush decrease, an alert issued by LPF at the time a 3-σ GCR flux decrease was reached around 16.00 UT, would have anticipated the geomagnetic disturbance observed at the Earth by several hours in case of appropriate baseline communication strategy. PDs aboard space missions allow for studying the energy dependence of GCR short-term depressions, their evolution and association with interplanetary structures better than allowed by the use of neutron monitor measurements only (see also Cane 2000, and references therein). The ICME tracking in space by Forbush decreases was also recently discussed in Witasse et al. (2017).

7. CONCLUSIONS

A PD aboard the ESA mission LPF allowed for the study of GCR short-term flux depressions above 70 MeV n^{-1} during the descending phase of the solar cycle N° 24. The majority of these depressions are recurrent and associated with corotating high speed solar wind streams. ICMEs and heliospheric current sheet crossing play a minor role. The average duration of GCR flux depressions observed aboard LPF are found of 9.2±5.0 days. Decrease, plateau and recovery average periods are 2.8±2.0 days, 1.3±1.2 days and 5.1±3.8 days, respectively. The average depression intensity is 5.1±2.5%.

The proton energy differential flux at the deep of a Forbush decrease observed on August 2, 2016 was obtained from the integral energy spectrum measurements carried out with LPF PD data and from those of neutron monitors placed in sites characterized by an increasing effective energy. Finally, it was shown that LISA-like and other missions in space, even if primarily devoted to difference science investigations, in some cases, may play the role of sentinels in monitoring the passage of magnetic structures that, when characterized by intense southern components of the magnetic field, induce geomagnetic activity.

The authors are grateful to the anonymous reviewer for his/her constructive comments and precious suggestions which helped us to greatly improve the manuscript. D. Telloni is financially supported by the Italian Space Agency (ASI) under contract I/013/12/0. Sunspot number and solar modulation parameter data were gathered from http://www.sidc.be/silso/home and http://cosmicrays.oulu.fi/phi/Phi_mon.txt, respectively. Data from Wind and ACE experiments were obtained from the NASA-CDAWeb website. We acknowledge the NMDB database (www.nmdb.eu) funded under the European Union's FP7 programme (contract no. 213007), and the PIs of individual neutron monitors for providing data. HCS crossing was taken from http://omniweb.sci.gsfc.nasa.gov./html/polarity/polarity_tab.html. This work has been made possible by the LISA Pathfinder mission, which is part of the space-science program of the European Space Agency. The French contribution has been supported by the CNES (Accord Specific de projet CNES 1316634/CNRS 103747), the CNRS, the Observatoire de Paris, and the University Paris-Diderot. E. P. and H. I. also acknowledge the financial support of the UnivEarthS Labex program at Sorbonne Paris Cité (ANR-10-LABX-0023 and ANR-11-IDEX-0005-02). The Albert-Einstein-Institut acknowledges the support of the German Space Agency, DLR. The work is supported by the Federal Ministry for

Economic Affairs and Energy based on a resolution of the German Bundestag (FKZ 50OQ0 501 and FKZ 50OQ1601). The Italian contribution has been supported by Agenzia Spaziale Italiana and Instituto Nazionale di Fisica Nucleare. The Spanish contribution has been supported by Contracts No. AYA2010-15709 (MICINN), No. ESP2013-47637-P, and No. ESP2015-67234-P (MINECO). M. N. acknowledges support from Fundacion General CSIC (Programa'ComFuturo). F.R. acknowledges an FPI contract (MINECO). The Swiss contribution acknowledges the support of the Swiss Space Office (SSO) via the PRODEX Program of ESA. L. F. acknowledges the support of the Swiss National Science Foundation. The United Kingdom groups acknowledge support from the United Kingdom Space Agency (UKSA), the University of Glasgow, the University of Birmingham, Imperial College, and the Scottish Universities Physics Alliance (SUPA). J. I. T. and J. S. acknowledge the support of the U.S. National Aeronautics and Space Administration (NASA). N. Korsakova acknowledges the support of the Newton International Fellowship from the Royal Society.

REFERENCES

Abe K. et al., 2016, ApJ, 822:65(16pp)
Adriani O. et al., 2011, ApJ, 742, 102
Antonucci F. et al., 2011, Class. Quantum Gravity, 28, 094001
Antonucci F. et al., 2012, Class. Quantum Gravity, 29, 124014
Araújo H. M. et al., 2005, Astropart. Phys., 22, 451
Armano M. et al., 2016, Phys. Rev. D, 116, 231101
Armano M. et al., 2017a, preprint (arXiv:1702.00786)
Armano M. et al., 2017b, Phys. Rev. Lett., 118, 171101
Badruddin and Kumar A., 2016, Solar Phys., 291, 559
Badruddin and Singh Y. P., 2006, Proc. ILWS Workshop, Eds. N. Gopalswamy and A. Bhattacharyya, Goa, India, 182
Bazilevskaya G. A., 2000, Sp. Sc. Rev., 94, 25
Beer J., 2000, Cosmic Rays and Earth J W Bieber, E Eroshenko, P Evenson, E O Flückiger and R Kallenbach eds. Space Science Review, (Elsevier), 93
Boella G. et al., 2001, J. Geophys. Res., 106, 29355
Burlaga F. L. et al., 1981, J. Geophys. Res., 86, 6673
Cane H. V., 2000, Sp. Sc. Rev., 93, 55
Cane H. V., Richardson I. G. and von Rosenvinge T. T., 1995, Proc. of the 24th International Cosmic-Ray Conference (ICRC) (Rome), 4, 872
Čalogović J. et al., 2008, Proc. of the International Astronomical Union (IAU), S257, 4, 425
Cañizares P. et al., 2011, Class. Quantum Gravity, 28, 094004
Clem J., Evenson P., 2004, J. Geophys. Res., 109, A07107
Emery B. A. et al., Solar Phys., 2011, 274, 399
Ferreira S. E. S., 2005, Adv. Sp. Res., 35, 586
Ferreira S. E. S., Potgieter M. S. and Scherer K., 2004, ApJ, 607, 1014
Forbush S. E., 1937, Phys. Rev., 51, 1108
Forbush S. E., 1954, J. Geophys. Res., 59, 525
Forbush S. E., 1958, J. Geophys. Res., 63, 651
Gil A., Alania M. V., 2010, Adv. Sp. Res., 45, 429
Gil A., Alania M. V., 2016, Sol. Phys., 291, 1877
Gil A. et al., 2017, Proc. of the 35th International Cosmic-Ray Conference (ICRC) (Busan), https://pos.sissa.it/301/032/pdf
Gleeson L. J. and Axford W. I., 1968, ApJ, 154, 1011
Grimani C., 2004, A&A, 418, 649
Grimani C. et al., 2004, Class. Quantum Gravity, 21, S629
Grimani C., 2007, A&A, 474, 339
Grimani C. et al., 2007, Proc. of the 30th International Cosmic-Ray Conference (ICRC) (Merida), 1, 485
Grimani C. et al., 2009, Class. Quantum Gravity, 26, 215004
Grimani C. et al., 2012, Class. Quantum Gravity, 29, 105001
Grimani C. et al., 2015, Class. Quantum Gravity, 32, 035001

Hajadas W. et al., 2004, Radiation and its effects on components and Systems RADECS 2003, Proceedings of the 7th European Conference 15-19 September 2003 in Noordwwijk, The Netherlands, Edited by K. Fletcher ESA SP-536 ESA/ESTEC, 635
Harang L., 1968, Planet. Space Sc., 16, 1095
Hofer M. Y. and Flückiger E. O., 2000, J. Geophys. Res., 105, 23-085
Iucci N. et al., 1979, Il Nuovo Cimento, 2C, 421
Laurenza M. et al., 2012, ApJ, 749, 167
Laurenza M. et al., 2014, ApJ, 781, 71
Lilensten J., Space Weather: Research towards applications in Europe, 2007, ISBN 978-1-4020-5446-4, Springer, 236
Lomb N., 1976, Ap&SS, 39, 447
Mateos I. et al., 2012, Journal of Physics: Conference Series, 363, 012050
McCracken K. G., Rao U. R. and Bucata R. P., 1966, Phys. Rev. Lett., 17, 928
McKibben R. B. et al., 1999, Sp. Sc. Rev., 89, 307
Nymmik R. A., 1999a, Proc. of the 26th International Cosmic-Ray Conference (ICRC) (Salt Lake City), 6, 268
Nymmik R. A., 1999b, Proc. of the 26th International Cosmic-Ray Conference (ICRC) (Salt Lake City), 6, 280
Papini P., Grimani C., Stephens A. S., 1996, Il Nuovo Cimento, 19, 367
Potgieter M. S., Langner U. W., 2004, Ap. J., 602, 993
Richardson I. G., Wibberenz G., Cane H. V., 1996, J. Geophys. Res., 101, 13483
Richardson I. G., 2004, Sp. Sc. Rev., 111, 267
Richardson I. G. and Cane H. V., 2010, Sol. Phys., 264, 189
Sabbah I., 2000, Geophys. Res. Lett., 27, 1823
Sabbah I., 2007, Sol. Phys., 245, 207
Sabbah I., Kudela K., 2011, J. Geophys. Res., 116, A04103
Scargle J. D., 1982, ApJ, 263, 835
Shaul D. N. A. et al., 2006, AIP Conf. Proc., 873, 172
Shikaze Y. et al., 2007, APh, 28, 154
Simpson J. A., 1954, Phys. Rev., 94, 426
Simpson J. A., 1998, Sp. Sc. Rev., 83, 169
Storini M., 1990, Il Nuovo Cimento, 13, 103
Strauss R. D. et al., 2011, J. Geophys. Res., 116, A12
Storini M., Iucci N., Pase S., 1992, Il Nuovo Cimento, 15, 527
Thakur N. et al., 2011, Proc. of the 32nd International Cosmic-Ray Conference (ICRC) (Beijing), 6, 280
Usoskin I. G., Solanki S. K. and Korte M., 2006, Geophys. Res. Lett., 33, L08103
Usoskin I. G., Bazilevskaya G., Kovaltsov G. A., 2011, J. Geophys. Res., 116, A02104
Usoskin I. G. et al., 2017, J. Geophys. Res. Space Physics, 122, 3875
Wiedenbeck M. E. et al., 2009, Proc. of the 31st International Cosmic-Ray Conference (ICRC) (Łódź)
Witasse O. et al., 2017, J. Geophys. Res. Space Physics, 122, 7865